Capture reactions in the ^{40,48}Ca + ^{197}Au and ^{40,48}Ca + ^{208}Pb systems

A. J. Pacheco, J. O. Fernández Niello, D. E. DiGregorio, M. di Tada, and J. E. Testoni
*TANDAR, Departamento de Física, Comisión Nacional de Energía Atómica, Avenida del Libertador 8250,
1429 Buenos Aires, Argentina*

Y. Chan, E. Chávez,* S. Gazes,† E. Plagnol,‡ and R. G. Stokstad
Nuclear Science Division, Lawrence Berkeley Laboratory, Berkeley, California 94720
(Received 22 November 1991)

Capture-fission cross sections for ^{40,48}Ca + ^{197}Au and ^{40,48}Ca + ^{208}Pb have been measured at beam energies ranging from 195 to 416 MeV. The fissionlike fragments were detected in a pair of position-sensitive multiwire proportional counters and were identified from measurements of position and time using two-body kinematics. The data taken at energies above the barrier (up to 2.4 times the Coulomb barrier) were analyzed in terms of the extra push model showing a strong dependence on the Ca isotope. This dependence was also observed at energies below the barrier, where the results have been interpreted using a schematic coupled-channel code.

PACS number(s): 25.70.$-$z, 25.70.Jj

I. INTRODUCTION

The study of nuclear reactions with heavy ions has revealed an interesting and rich interplay of nuclear structure and reaction mechanism [1]. Basically, the barrier for fusion governs the size and energy dependence of the cross sections. Nuclear structure, on both a macroscopic and microscopic level, determines the barrier. The macroscopic aspects (Coulomb repulsion, liquid-drop-like nuclear forces, moments of inertia) set the global behavior. For example, when the colliding nuclei are highly charged, fusion at the barrier is inhibited and extra energy is required to force the nuclei together [2]. In this case, it may even be questionable whether fusion, in the usual sense of compound-nucleus formation, does indeed occur. It has been proposed that if the dynamical evolution does not drive the dinuclear complex beyond the unconditional saddle point, then a mononucleus may be formed. Although this mononucleus is indistinguishable from the true compound nucleus from the standpoint of its identity as a nuclear species, their respective subsequent evolutions and decays may differ substantially. Both types of processes fall in the general category of capture reactions.

On top of these general aspects come interesting second-order effects. For example, in the case of very heavy nuclei it appears that shell effects can influence cross sections at bombarding energies above the barrier. Other second-order effects, which can be greatly magnified if the bombarding energy is well below the barrier, are intimately connected with nuclear structure and arise from collective nuclear phenomena such as deformation [3,4] and vibration, and from microscopic single-particle properties such as nucleon transfer [5,6].

Basic to an understanding of these processes are measurements that can single out particular effects. For example, the effect of deformation is examined by comparing targets that differ in this aspect but are otherwise similar, as in the case of the samarium isotopes [3,4]. Similarly, the tin nuclei are excellent for studying the effects of vibration [7,8]. It is also interesting to examine cases in which the effects of nuclear structure such as rotations and vibrations are minimized. This should help test our understanding of the underlying nuclear potential that is the basis for the one-dimensional calculations of nuclear fusion. Since reactions of doubly magic projectile and target nuclei are the closest approximation to this ideal situation, we have chose for study the systems ^{40,48}Ca + ^{208}Pb.

A second factor influencing the choice of projectile and target in the present work is the threshold at which the extra push becomes important, and which is known to lie in the vicinity of the Ca + Pb systems. The availability of the projectiles ^{40}Ca and ^{48}Ca enables one to vary the effective fissility without the large change in barrier height accompanying a change in projectile charge. Thus, we have undertaken an experimental study of the capture reactions of ^{40,48}Ca on targets of ^{197}Au and ^{208}Pb at energies above and below the barrier.

II. EXPERIMENTAL PROCEDURE

The experiments were performed at the Lawrence Berkeley Laboratory. Beams of ^{40}Ca and ^{48}Ca with energies between 195 and 416 MeV were provided by the ECR ion source and the 88-Inch Cyclotron. This energy range corresponds to center-of-mass energies from 0.93 to 2.41 times the Coulomb barriers. The targets were self-

---

*Present address: Physics Division, Oak Ridge National Laboratory, Oak Ridge, TN 37831.
†Present address: Department of Physics and Astronomy, University of Rochester, Rochester, NY 14627.
‡Present address: GANIL, B.P. 5027, F-14021, Caen CEDEX, France.

supporting foils of Au or isotopically enriched [208]Pb with thicknesses between 200 and 250 $\mu g/cm^2$. The fragments produced in the binary collisions were detected by a pair of multiwire proportional counters, each with an active area of 16×16 cm^2, placed at either side of the beam on the plane of the scattering chamber. The distances from these counters to the target were 40 cm ("master detector") and 20 cm ("slave detector"), respectively. These detectors measured the position and the time of arrival of the detected particles. Since they were operated in coincidence mode, their angular positions (θ_M and θ_S) were chosen so as to maximize the detection efficiency for the desired range of exit-channel configurations, as defined by the mass partition (i.e., by the masses of the fragments detected by the master and slave counters, M_M and M_S, respectively), and the total kinetic energy loss (TKEL). The normalization for absolute cross sections was obtained by monitoring the Rutherford scattering from the target with a surface-barrier detector located at $11.8°$ from the beam. An additional solid-state detector was placed behind one of the multiwire counters in order to check the deduced kinetic energies for a portion of the coincidence events.

The data were recorded on magnetic tape in the form of multiparameter events. Each event consisted of, essentially, the x,y position of each particle and the difference between their times of arrival at the corresponding counters. The position calibrations were made with a [252]Cf source after appropriate masking of the detectors. The time calibrations were performed both with a time calibrator and from the known kinematics for elastic scattering.

The data reduction was done at the TANDAR Laboratory in Buenos Aires. For every event, the coordinates of
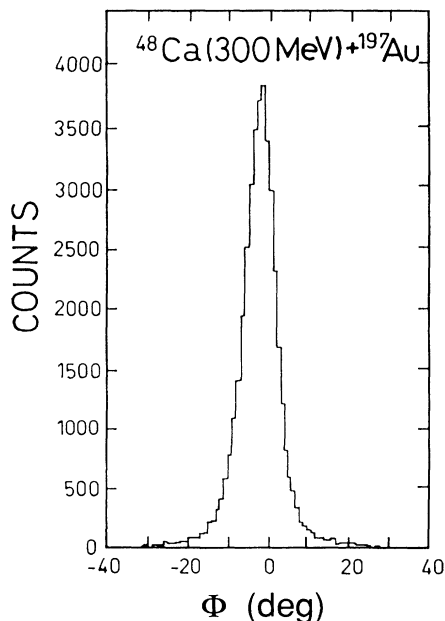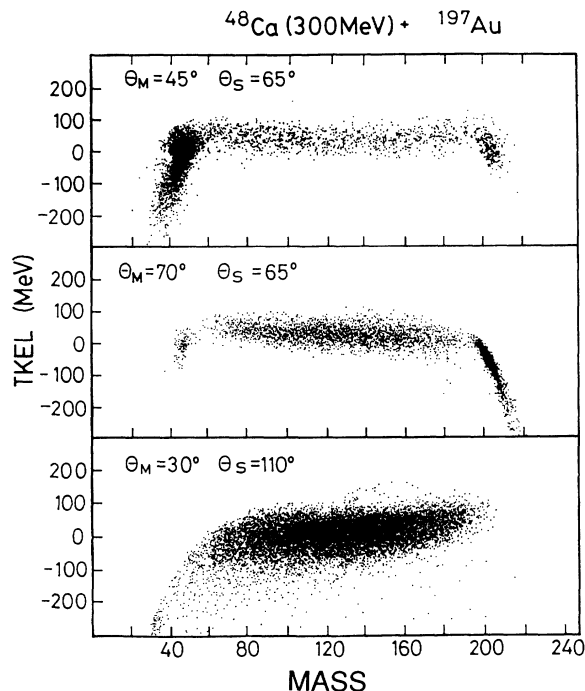

FIG. 2. Total kinetic energy loss (TKEL) vs mass of the fragment detected in the master detector. Each frame qualitatively illustrates the fact that different geometrical configurations optimize the detection of fragments corresponding to a given mass region; projectilelike fragments (upper frame), targetlike fragments (middle frame), intermediate-mass fragments (lower frame).

the points where the coincident fragments hit each detector were transformed to the corresponding azimuthal angle ϕ' and polar angle θ', taken with respect to the beam direction. A measurement of the azimuthal angles provides a direct check of the coplanarity of the reaction. An example of distribution of the difference between azimuthal angles $(\theta_1+\theta_2-\pi)$ is shown in Fig. 1; the peak centered near $0°$ indicates the dominance of binary reactions. By gating on these events, the kinematics of the collision could be reconstructed to yield M_M, M_S, TKEL, and the center-of-mass angles (θ and ϕ). For the systems investigated here, the geometric configuration corresponding to $\theta_M=30°$, $\theta_S=110°$ showed the maximum efficiency for intermediate mass fully, relaxed fissionlike events, and was therefore used over the entire range of bombarding energies for all the systems. A few runs were also taken at $\theta_M=55°$, $\theta_S=60°$ in order to emphasize elastic and quasielastic scattering. For [48]Ca+[197]Au at 300 MeV a more complete angular distribution was measured by taking data at several other pairs of θ_M,θ_S values. As an example of the kind of coverage that could be obtained, Fig. 2 shows mass versus TKEL plots for $(\theta_M,\theta_S)=(45°,65°)$, $(70°,65°)$, and $(30°,110°)$.

FIG. 1. Spectrum of the differences between azimuthal angles $(\theta_1+\theta_2-\pi)$ (coplanarity) of the outgoing fragments (see text).

III. DETERMINATION OF CAPTURE CROSS SECTIONS

Differential cross sections for capture-fission processes were deduced by integration of the mass spectra over the

broad bump centered at symmetry (i.e., excluding the quasielastic peaks), for a rectangular gate defined by $\theta\pm\Delta\theta$, $\phi\pm\Delta\phi$. The azimuthal width $\Delta\phi$ was restricted essentially by the active area of the detector, while $\Delta\theta$ was taken equal to 2.5° around the optimum value θ that would guarantee 100% efficiency for coincidence measurements of fission fragments in the regions of interest for both mass and TKEL.

These differential cross sections $d\sigma(\theta)/d\Omega$ (averaged over the angular region under consideration) were used to deduce the total capture cross sections σ_c by

$$\sigma_c = (\Delta\phi\mathcal{F})^{-1}\frac{d\sigma}{d\Omega}(\theta) . \tag{1}$$

In this expression, $\mathcal{F}$ is given by

$$\mathcal{F} = \int_{\theta-\Delta\theta}^{\theta+\Delta\theta} W(x)\sin x \, dx , \tag{2}$$

where $W(x)$ is the angular distribution so normalized that $2\pi\int_0^\pi W(x)\sin x \, dx = 1$. The simplest assumption that can be made is that the fission fragments are emitted in a plane perpendicular to the total angular momentum vector, in which case the angular distribution is given by

$$W(\theta) = (2\pi^2\sin\theta)^{-1} . \tag{3}$$

In an attempt to consider more realistic situations, we have calculated the angular distributions using the following expression taken from Ref. [9]:

$$W(\theta) \propto \sum_{I=0}^{\infty} \frac{(2I+1)^2 T_I \exp[-(I+\frac{1}{2})^2\sin^2\theta/4K_0^2]J_0[i(I+\frac{1}{2})^2\sin^2\theta/4K_0^2]}{\text{erf}[(I+\frac{1}{2})/(2K_0^2)^{1/2}]} . \tag{4}$$

Here, T_I is the transmission coefficient associated with the total angular momentum I, and K_0 is proportional to the variance of the distribution of the component along the axis of decay. Expression (4) is an approximation to the exact relation that holds for the fission decay of an equilibrated system formed in a reaction in which the orbital angular momentum is much larger than the spins of the projectile and target nuclei. It can be shown that this expression depends almost exclusively on the ratio $K_0^2/\langle I^2\rangle$.

For the calculation of $\langle I^2\rangle$ we assumed that the total angular momenta of the compound systems were distributed according to the sharp cutoff model. This assumption is not expected to hold as the energies approach or decrease below the barrier. For these cases, increasingly broader spin distributions are known to contribute to the fusion process [10,11]. In an attempt to take this effect into account the spin distribution for subbarrier energies were calculated using the schematic coupled-channel code CCFUS [12] (it was also verified that even for the smallest energies above the barrier, the difference between the calculated values of $\mathcal{F}$ using the crude method or the more realistic spin distributions predicted by CCFUS were negligible).

For K_0 we used

$$K_0^2 = \mathcal{F}_{\text{eff}}T/\hbar^2 , \tag{5}$$

where $\mathcal{F}_{\text{eff}}$ is the effective moment of inertia and T is the temperature. Based on the systematics as a function of $\langle I^2\rangle$ for the similar systems ^{28}Si+^{208}Pb and ^{32}S+^{197}Au,^{208}Pb (Ref. [13]), we used for all our cases a value of 0.65 for $\mathcal{F}_0/\mathcal{F}_{\text{eff}}$ were $\mathcal{F}_0$ is the moment of inertia of the spherical compound system.

Finally, the nuclear temperature was calculated from

$$T^2 = 8.5(E^* - E_{\text{rot}} - B_f)/A , \tag{6}$$

where E^* is the excitation energy, E_{rot} is the rotational energy of the fissioning complex, and B_f is the fission barrier, which we have neglected for these heavy systems.

In order to estimate the rotational energy we assumed that, for the heavy compound systems under consideration, the saddle-point shapes do not differ greatly from those of the corresponding ground states. Hence, assuming small quadrupole deformations we obtain

$$E_{\text{rot}} = E_{\text{rot}}^{(0)}\left[1 - \frac{\mathcal{F}_0}{3\mathcal{F}_{\text{eff}}}\right] , \tag{7}$$

where $E_{\text{rot}}^{(0)}$ is the rotational energy classically associated with the equivalent spherical system. This energy was calculated assuming a moment of inertia given by $0.014A^{5/3}\hbar^2$/MeV (obtained from a radius parameter $r_0 = 1.2$), and using the values of $\langle I^2\rangle$ and of $\mathcal{F}_0/\mathcal{F}_{\text{eff}}$ as described above.

The angular distribution calculated with expression (4) was numerically normalized and integrated [see Eq. (2)] in order to obtain the relationship between differential and total cross sections [see Eq. (1)].

Figure 3 shows four cases of calculated angular distributions. The solid and dashed curves correspond to a $1/\sin\theta$ distribution [Eq. (3)], and to the case $K_0^2/\langle I^2\rangle \to \infty$ (i.e., an isotropic distribution), respectively The dotted and dash-dotted curves indicate the angular distributions which result from applying the above-described procedure to the reaction ^{48}Ca (224.3 MeV) $+^{197}$Au ($K_0^2/\langle I^2\rangle = 0.13$) and to ^{48}Ca (416 MeV)$+^{208}$Pb ($K_0^2/\langle I^2\rangle = 0.017$). Since the correction factor required to transform differential cross sections to total cross sections is proportional to the integral over the region indicated by the arrows [see Eqs. (1) and (2)], it is apparent from Fig. 3 that the angular position of the detectors makes the results relatively insensitive to large changes in the overall angular distributions, thus minim-
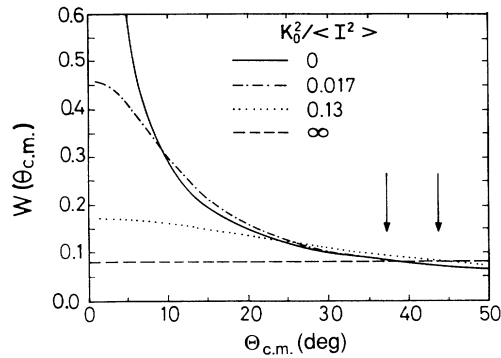
FIG. 3. Normalized theoretical angular distributions for different ratios, $K_0^2/\langle I^2 \rangle$. The arrows indicate the boundaries of the integral in Eq. (2) required in the determination of total capture cross sections (see text for details).

izing systematic errors arising from this factor to less than 2%.

There are several other sources of uncertainties in the determination of capture cross sections. Random errors arising from counting statistics include the effect of the uncertainty in the separation between quasielastic and capture events. Systematic errors, such as those affecting the determination of the distances and angular positions of the detectors may affect event-by-event calculations but do not have a direct impact on integrated quantities such as capture cross sections. On the other hand, angular shifts may affect the calculated factor for the angular-distribution correction. The largest of all the contributions to the systematic error comes from an uncertainty in the determination of the angular position and solid angle subtended by the monitor detector. Considering all the above mentioned sources, a total systematic uncertainty of approximately 12% has been estimated.

IV. RESULTS

Figure 4 compares experimental angular distributions in the forward hemisphere for ^{48}Ca (300 MeV) $+^{197}$Au (i.e., one of the cases for which data were taken at several master-slave configurations), with those calculated following the procedure described in the previous section in connection with Eq. (4). Each graph corresponds to one of the 15-u wide bins within the intermediate-mass region. The quality of the agreement is fairly independent of the mass region under consideration. The behavior of the total capture cross sections for the four systems as a function of center-of-mass energies is summarized in Figs. 5 and 6 and Table I. The data are plotted linearly (Fig. 5) and logarithmically (Fig. 6) in order to emphasize the most salient trends above and below the barrier, respectively. Figure 5 also includes the capture cross sections obtained in Ref. [14], for the ^{48}Ca$+^{208}$Pb reaction, which appear to be systematically lower than those measured at the highest energies in the present work. Qualitatively, the excitation functions show the expected fall as the energy decreases below the Coulomb barrier. Above the barrier, the measured cross sections are lower than

predicted by the "touching" limit for which all the partial waves up to the grazing angular momentum contribute to the capture process.

A. Above the barrier

The difference between experimental and touching-limit capture cross sections is not unexpected in the light of our current knowledge about collisions between heavy nuclei. Indeed, the "missing" cross section has been interpreted as evidence for the need of a nonzero radial velocity (extra push) at the point of contact between the two nuclei in order to form a mononucleus (capture reaction). This feature, among others, may be directly derived from the dynamical theory of heavy-ion reactions developed by Swiatecki. Since the model and its application to capture processes have been extensively discussed elsewhere [2,15,16] we shall review only a few basic points.
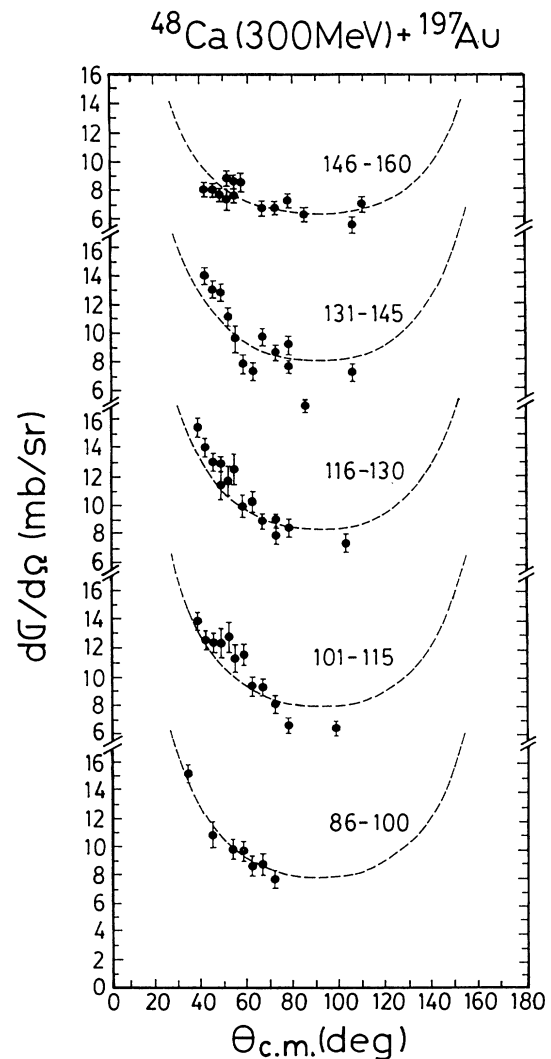

FIG. 4. Experimental angular distributions corresponding to different mass regions. The dashed lines are calculations following the procedure described in the text.
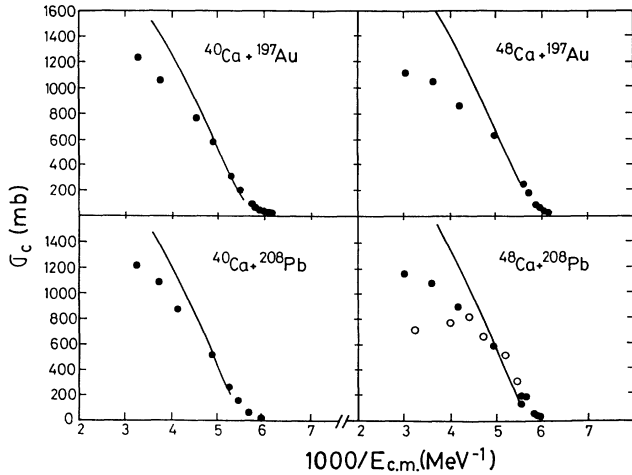
FIG. 5. Capture cross sections vs the inverse of the center-of-mass energies. Solid lines correspond to calculations assuming a "touching" condition. Open symbols correspond to the data of Ref. [14].

The main result of the model is that capture reactions for a given projectile-target system at a given center-of-mass energy $E_{c.m.}$ will take place for all the partial waves up to a maximum value l that guarantees a minimum value of the radial velocity at contact. This minimum value is, in turn, a function of l. This may be expressed in terms of the capture cross section σ_c through the following condition:

$$E_{c.m.} - V - \frac{\sigma_c(E_{c.m.})E_{c.m.}}{\pi R^2} = E_x(l) ,\qquad (8)$$

where V and R are the value of the nuclear potential at contact and the interaction radius, respectively, and E_x is the extra push required at the limiting angular momentum. [By setting the right-hand side of Eq. (8) equal to zero one recovers the usual touching condition.] The theory also predicts the following dependence of the extra push on the reaction system and on the angular momentum:
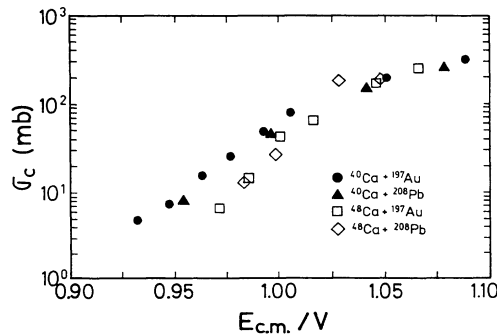

FIG. 6. Near-barrier capture cross sections vs center-of-mass energies in units of the barrier heights for each system ($V=174.9$, 169.4, 178.2, and 174.3 MeV for ^{40}Ca$+^{197}$Au, ^{48}Ca$+^{197}$Au, ^{40}Ca$+^{208}$Pb, and ^{48}Ca$+^{208}$Pb, respectively).

$$E_x(l) = E_{ch}a^2[(x - x_{th}) + (fl/l_{ch})^2]^2 .\qquad (9)$$

Here, E_{ch} is a characteristic energy, l_{ch} is a characteristic angular momentum, and x is the effective fissility parameter. These three quantities depend upon the reaction system through the atomic masses and atomic numbers of the projectile and target nuclei. Expression (9) also contains three constants (x_{th}, a, and f) which may be taken as free parameters when adjusting the theory to the experimental data. The parameter x_{th} defines the threshold fissility above which an extra push is required in order to induce a capture reaction in a central collision. The parameter a governs the rate at which this extra push for central collisions increases with increasing fissility. Finally, f connects the extra-push energy with l, and may be roughly interpreted as the fraction of the total angular momentum that remains in the orbital motion.

The analysis of our data in terms of the extra-push model proceeded as follows: The calculation of E_x for the four measured reaction systems was performed by applying Eq. (8), using a folded Yukawa potential. Following the procedure applied by Toke et al. [17] and Shen et al. [18] we plotted the square root of the experimental extra-push energies in units of E_{ch} as a function of the square of the limiting angular momentum in units of l_{ch}, as shown in Fig. 7. According to expression (9), by fitting the data with a straight line one obtains af^2 from the slope and $a(x - x_{th})$ from the intercept. The quantity $a(x - x_{th})$ is proportional to the square root of the extra push required in a central collision. In our case, the data points in Fig. 7 clearly group in two families, each of them characterized by the projectile nucleus. At this point we have considered several possibilities. First, we extracted the parameters of the single straight line that best fits the data for the four systems. Although this average procedure is consistent with the idea of truly "universal" constants, it appears rather unphysical given the experimental evidence from this work. A second approach was to perform independent fits to each of the two projectile-dependent groups of points, as indicated by the lines in Fig. 7. Finally each projectile-target combination was considered individually. The values of the adjustable parameters corresponding to these three cases are summarized in Table II. The corresponding errors were estimated from the largest variations in the slopes of each of the straight lines that would still produce acceptable fits. The effective fissilities for each system, calculated following the procedure given by Bass [19] and assuming that the mass and charge partitions correspond either to the entrance channel x_{Bass} or to charge-to-mass equilibrium $(x_{Bass})_{eq}$ are also shown. The experimental values of $\sqrt{E_x(l=0)/E_{ch}}$ are in all cases close to zero, and this is consistent, at least qualitatively, with the fact that the theoretical expectations for the effective fissilities are very close to the theoretical threshold value, $x_{th}=0.7$. Figure 8 displays the deduced values of $\sqrt{E_x(l=0)/E_{ch}}$ as a function of $(x_{Bass})_{eq}$. It has been shown that the use of these equilibrium fissilities gives results that are more

TABLE I. Total capture cross sections as a function of center-of-mass energy.

System	$E_{c.m.}$ (MeV)	σ_{cap} (mb)	System	$E_{c.m.}$ (MeV)	σ_{cap} (mb)
^{40}Ca+^{197}Au	162.75	4.6±0.4	^{40}Ca+^{208}Pb	169.67	7.88±0.46
	165.41	7.1±0.4		177.14	45.5±1.5
	168.16	14.7±0.4		185.19	138±4
	170.57	25.2±0.6		191.81	242±4
	173.31	47±2		207.92	494±5
	175.55	73±3		246.08	856±9
	183.53	178±6		272.83	1071±16
	190.10	290±8		313.51	1200±18
	206.06	554±6			
	222.68	747±8			
	270.40	1040±12			
	310.71	1215±21			
^{48}Ca+^{197}Au	164.35	6.5±0.3	^{48}Ca+^{208}Pb	171.03	13.3±0.8
	166.69	14.3±1.2		173.71	26.2±1.9
	169.26	42.1±2.7		178.83	165±8
	171.91	60±4		182.24	141±10
	176.98	155±7		205.16	569±9
	180.36	227±6		243.18	872±17
	203.03	605±11		281.37	1064±11
	240.66	837±13		338.08	1141±17
	278.45	1028±11			
	334.58	1098±15			

consistent with the predicted linear relation with $\sqrt{E_x(l=0)}/E_{ch}$ [18]. The data points from the present work are included together with those of Ref. [18]. The fissilities in this figure were calculated following the prescription given by Bass [19], and assuming equilibrium charge-to-mass ratios for the entrance-channel mass asymmetries.
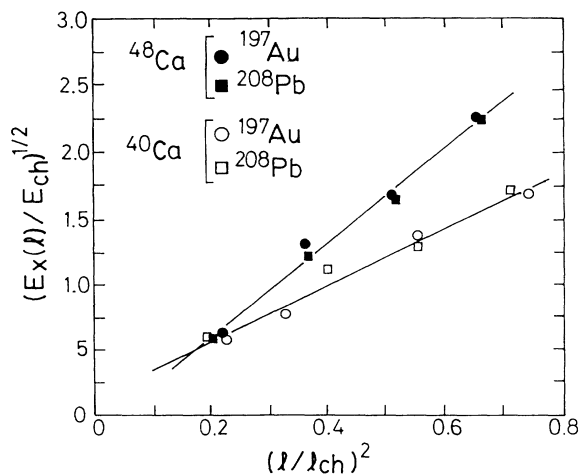
Because our data points are in qualitative agreement

FIG. 7. Square root of the experimental extra-push energies as a function of the square of the limiting angular momentum. The straight lines are fits to each of the two families of data points using expression (9). Each family of points is characterized by the projectile nucleus.

with the complete systematics presented in Ref. [18], we have chosen to use their values $a = 7.3$ and $x_{th} = 0.62$ rather than attempting to derive new ones. From this and Table II we can obtain the values of f that best fit our data. These values are displayed in Table III, together with the calculated ratios between the orbital and total angular momenta corresponding to the rigid rotation (sticking) and rolling regimes determined by the entrance-channel mass asymmetry. For the ^{48}Ca+^{208}Pb system f is larger than the value determined by Toke et al. ($f = 0.65$), although the latter was obtained using different values of a and x_{th}. The results of Table III show that the experimental values of f are systematically higher than rigid-rotation predictions and that they increase with decreasing mass asymmetry. Although this dependence is in qualitative agreement with the sticking limit, the sudden increase in going from ^{40}Ca to ^{48}Ca seems to go beyond the expected smooth trend. If this difference between the two projectile nuclei is significant it might suggest that it is harder to transfer spin to the ^{48}Ca nucleus, thus leaving a larger fraction of the total angular momentum in orbital motion. Due to possible systematic uncertainties in the determination of the absolute values of f, it is difficult to draw firm conclusions. The observed behavior could be attributed, for example, to one of the following situations: (i) rotational degrees of freedom evolve toward but do not attain rigid rotation (as suggested by the dependence of f on mass asymmetry) and (ii) the relevant mass asymmetry to be considered for the comparison with the parameter f included in the present model is somewhere in between those of the entrance and exit channels, in which case the distinction between rolling and sticking tends to disappear.

TABLE II. Slopes and intercepts (columns 2 and 3, respectively) of the best linear fits to different sets of the data points shown in Fig. 7 (see text). The effective fissilities according to Bass [19] for all the four systems considering both entrance-channel (column 4) and charge-to-mass equilibrated (column 5) partitions are shown.

System	af^2	$a(x-x_{th})$	x_{Bass}	$(x_{Bass})_{eq}$
Four systems	2.67	0.09		
^{40}Ca	2.15±20	0.14±8		
^{48}Ca	3.59±35	−0.12±9		
^{40}Ca$+^{197}$Au	2.21±20	0.08±8	0.740	0.644
^{40}Ca$+^{208}$Pb	2.08±20	0.20±10	0.751	0.645
^{48}Ca$+^{197}$Au	3.66±35	−0.12±8	0.688	0.671
^{48}Ca$+^{208}$Pb	3.54±35	−0.12±8	0.697	0.674

B. Below the barrier

Since the extra-push model is essentially classical, the data that we have dealt with so far are those taken at energies above the barrier. Capture cross sections were also measured down to energies ranging from about 93% to 98% of the corresponding barriers (see Fig. 6). As was the case for the angular-momentum fraction f extracted from the data above the barrier, the sub-barrier results tend to group according to the projectile while they are rather insensitive to the target nucleus. Indeed, the ^{48}Ca excitation functions for both targets exhibit a steeper fall than those of the ^{40}Ca projectile.

In order to interpret the sub-barrier behavior of the capture cross sections we have performed schematic coupled-channel calculations using the code CCFUS. Although from a macroscopic point of view capture and fusion reactions may not proceed through the same dynamical paths, this approach assumes that the coupling to selected inelastic and transfer channels may aid the formation of a mononucleus.

The code CCFUS uses the nuclear potential of Christensen and Winther [20], and it considers an adjustable parameter (dV) that adds to the potential depth. This parameter was chosen so that the cross sections above the barrier were reproduced as closely as possible. For that purpose we took as a reference the cross sections predicted by the touching condition rather than the experimental values, since it cannot be expected that these coupled-channel calculations be able to reproduce results that require the concept of an extra push.

The channels considered in the calculations at energies below the barrier were the inelastic excitations to the low-lying 3^- and 2^+ states of ^{40}Ca, ^{48}Ca, and ^{208}Pb, and the low-lying $\frac{5}{2}^+$ and $\frac{7}{2}^+$ of ^{197}Au, as well as the transfer of one and two neutrons from the projectile to the target. The results are displayed in Fig. 9 for the four reaction systems. The solid curves correspond to no coupling, the dash curves include all the inelastic excitations, and the dash-dotted curves were obtained by coupling all inelastic and transfer channels. In all cases the data points lie well above any of the calculated curves. Due to the schematic nature of CCFUS, this may not be conclusive as to whether the coupling to these inelastic and transfer channels is enough to explain the observed sub-barrier enhancement. In any case, these calculations may be useful in establishing a few general trends. The largest contribution to the enhancement comes from the inelastic excitations, while the influence of the neutron transfer channels is much more important for ^{40}Ca than for ^{48}Ca.
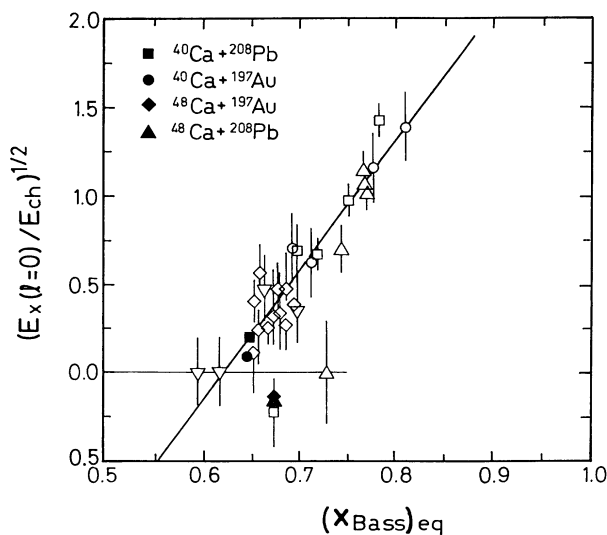

FIG. 8. Square root of the experimental extra-push energies for central collisions as a function of the effective fissility assuming charge equilibration. Open symbols are taken from the systematics presented in Ref. [18]. The solid line correspond to expression (9) for $l=0$, using $a=7.3$ and $x_{th}=0.62$.

TABLE III. Experimental values of the parameter f compared to the corresponding predictions for the rigid-rotation and rolling regimes, as a function of the mass asymmetry for the studied systems. These experimental values were obtained assuming $a=7.3$ and $x_{th}=0.62$.

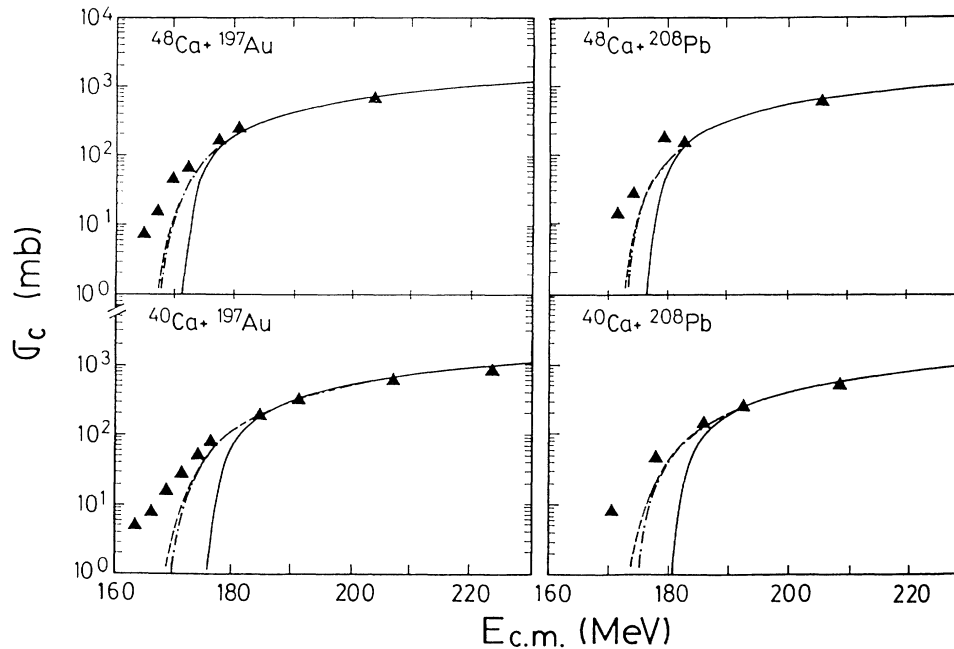| System	Mass asymmetry	f_{exp}	$f_{rigid\ rot.}$	$f_{rolling}$
^{40}Ca$+^{197}$Au	0.662	0.55±0.03	0.50	0.71
^{40}Ca$+^{208}$Pb	0.677	0.53±0.03	0.49	0.71
^{48}Ca$+^{197}$Au	0.608	0.71±0.03	0.54	0.71
^{48}Ca$+^{208}$Pb	0.625	0.70±0.03	0.53	0.71

FIG. 9. Near-barrier fusion cross sections for the four reaction systems compared to various schematic coupled-channel calculations using the code CCFUS (see text).

V. SUMMARY

Capture-fission cross sections for ^{40,48}Ca$+^{197}$Au and ^{40,48}Ca$+^{208}$Pb were measured at energies ranging from about 0.95 to 2.4 times the Coulomb barriers. The experimental method was based on the detection of both exit-channel fragments in two position-sensitive multiwire proportional counters. After checking each event for co-planarity (thus establishing its binary nature), the exit-channel mass partition, total kinetic energy loss, and center-of-mass angle were calculated by applying the kinematical-coincidence technique. Total capture cross sections were deduced from measurements performed at one geometrical configuration after applying corrections for the angular distributions. These were calculated using a theoretical expression for the fission decay of an equilibrated system. At one bombarding energy the calculations were compared to a more complete angular distribution measured in the forward hemisphere.

At energies above the barrier, experimental cross sections fall below the calculations performed under the assumption that all partial waves up to the grazing angular momentum undergo capture, and the magnitude of the discrepancy increases with increasing energy. A quantitative analysis based on Swiatecki's model shows that these results are consistent with the requirement of an extra push in the radial direction for the occurrence of capture. The adjustable parameters of the model depend quite strongly on the light reaction partner but are relatively insensitive to the heavy nucleus. The extra push as a function of angular momentum increases faster for ^{48}Ca than for ^{40}Ca induced reactions both for ^{197}Au and ^{208}Pb. Also, the extra push needed for central collisions is very close to zero for these four systems, in good agreement

with the expectations from systematics. Within the framework of the model, one can also extract the partition of the total angular momentum between intrinsic and orbital degrees of freedom. The dependence of this partition on mass asymmetry shows a qualitative behavior consistent with rigid rotation although the orbital component is, within experimental uncertainties, larger than expected for this rotational regime.

At near- or below-barrier energies capture excitation functions also seem to depend almost exclusively on the light nucleus. For both heavy targets sub-barrier capture enhancement is more important for ^{40}Ca than for ^{48}Ca. This behavior, which might be attributed to a greater "magicity" of the latter, is qualitatively reproduced by calculations using the schematic coupled-channel code CCFUS, regardless of the specific inelastic and/or transfer channels that are selected for coupling. The individual contribution of inelastic channels is much more significant than transfer channels. In all cases, however, the absolute magnitude of the enhancement is underestimated by the calculations.

[1] W. Reisdorf, in Proceedings of the International Conference on Nuclear Physics, Harrogate, 25–30 August 1986, edited by J. L. Durell, J. M. Irvine, and G. C. Morrison (IOP Publishing Ltd Techno House, Bristol, England, 1987).

[2] W. J. Swiatecki, Phys. Scr. **24**, 113 (1981).

[3] R. G. Stokstad, Y. Eisen, S. Kaplanis, D. Pelte, U. Smilansky, and I. Tserruya, Phys. Rev. C **21**, 2427 (1980).

[4] D. E. DiGregorio, J. O. Fernandez Niello, A. J. Pacheco, D. Abriola, S. Gil, A. O. Macchiavelli, J. E. Testoni, P. R. Pascholati, V. R. Vanin, R. Liguori Neto, N. Carlin Filho, M. M. Coimbra, P. R. S. Gomes, and R. G. Stokstad, Phys. Lett. B **176**, 322 (1986).

[5] K. E. Rehm, F. L. H. Wolfs, A. M. van der Berg, and W. Henning, Phys. Rev. Lett. **55**, 280 (1985).

[6] R. A. Broglia, C. H. Dasso, S. Landowne, and G. Pollarolo, Phys. Lett. **133B**, 34 (1983).

[7] W. Reisdorf, F. P. Hessberger, K. D. Hildenbrand, S. Hofmann, G. Munzenberg, K.-H. Schmidt, J. H. R. Schneider, W. F. W. Schneider, K. Summerer, G. Wirth, J. V. Kratz, and K. Schlitt, Nucl. Phys. **A438**, 212 (1985).

[8] P. Jacobs, Z. Fraenkel, G. Mamane, and I. Tserruya, Phys. Lett. B **175**, 271 (1986).

[9] J. R. Huizenga, A. N. Behkami, and L. G. Moretto, Phys. Rev. **177**, 1826 (1969).

[10] S. Gil, R. Vandenbosch, A. J. Lazzarini, D.-K. Lock, and A. Ray, Phys. Rev. C **31**, 1752 (1985).

[11] P. J. Nolan, D. J. G. Love, A. Kirwan, D. J. Unwin, A. H. Nelson, P. J. Twin, and J. D. Garrett, Phys. Rev. Lett. **54**, 2211 (1985).

[12] C. H. Dasso and S. Landowne, Comput. Phys. Commun. **46**, 187 (1987).

[13] B. B. Back, R. R. Betts, J. E. Gindler, B. D. Wilkins, S. Saini, M. B. Tsang, C. K. Gelbke, W. G. Lynch, M. A. McMahan, and P. A. Baisden, Phys. Rev. C **32**, 195 (1985).

[14] R. Bock, Y. T. Chu, M. Dakowski, A. Gobbi, E. Grosse, A. Olmi, H. Sahn, D. Schwalm, U. Lynen, W. Muller, S. Bjornholm, H. Esbensen, W. Wolfli, and E. Morenzani, Nucl. Phys. **A388**, 334 (1982).

[15] W. J. Swiatecki, Nucl. Phys. **A376**, 275 (1982).

[16] S. Bjornholm and W. J. Swiatecki, Nucl. Phys. **A391**, 471 (1982).

[17] J. Toke, R. Bock, G. X. Dai, A. Gobbi, S. Gralla, K. D. Hildenbrand, J. Kuzminski, W. F. J. Muller, A. Olmi, H. Stelzer, B. B. Back, and S. Bjornholm, Nucl. Phys. **A440**, 327 (1985).

[18] W. Q. Shen, J. Albinski, A. Gobbi, S. Gralla, K. D. Hildenbrand, N. Herrmann, J. Kuzminski, W. F. J. Muller, H. Stelzer, and J. Toke, Phys. Rev. C **36**, 115 (1987).

[19] R. Bass, Nucl. Phys. **A231**, 45 (1974).

[20] P. R. Christensen and A. Winther, Phys. Lett. **65B**, 19 (1976).